# *A whole pattern iterative refinement method for powder X-ray diffraction spectra of two-phase coherent alloys*

**P. A. Ferreirós & G. H. Rubiolo**

**Journal of Materials Science**
Full Set - Includes `Journal of Materials Science Letters'

ISSN 0022-2461
Volume 53
Number 4

J Mater Sci (2018) 53:2802-2811
DOI 10.1007/s10853-017-1682-5

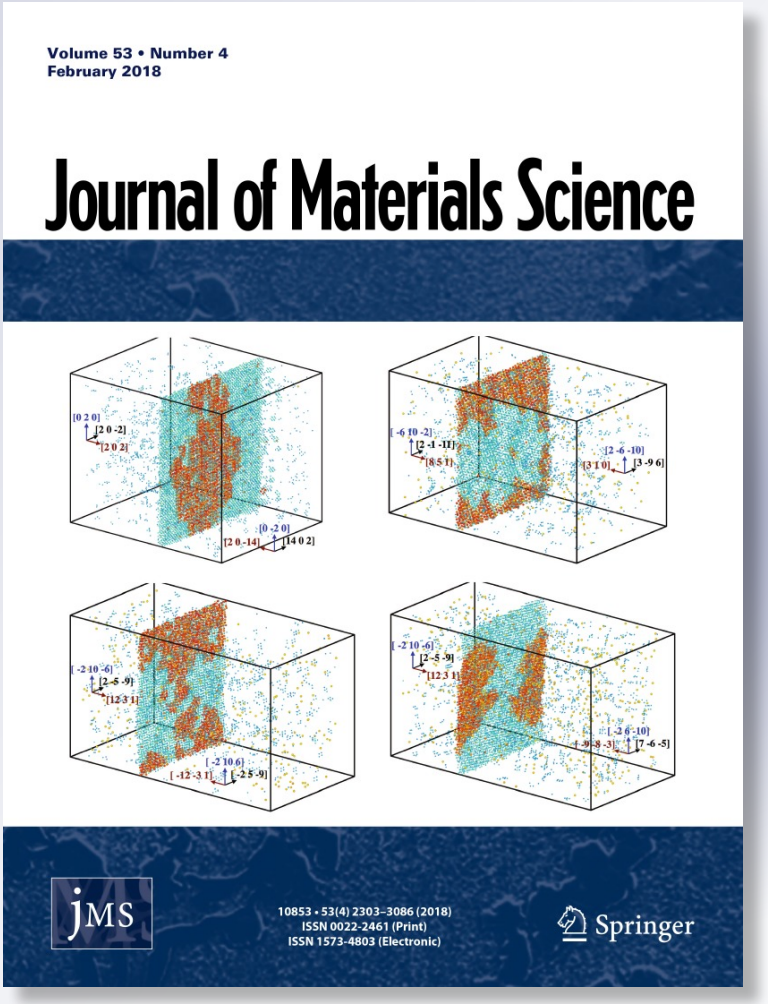


Springer

*J Mater Sci* (2018) 53:2802–2811

Metals

# A whole pattern iterative refinement method for powder X-ray diffraction spectra of two-phase coherent alloys

P. A. Ferreirós[1,2,*] and G. H. Rubiolo[1,3]

[1] Gerencia Materiales (GAEN), Comisión Nacional de Energía Atómica (CNEA), Instituto Sabato, Universidad Nacional de San Martín (UNSAM), Av. Gral. Paz 1499, B1650KNA San Martín, Buenos Aires, Argentina
[2] Facultad Regional General Pacheco (UTN-FRGP), Universidad Tecnológica Nacional, Av. Hipólito Yrigoyen 288, B1617FRP Gral. Pacheco, Buenos Aires, Argentina
[3] Consejo Nacional de Investigaciones Científicas y Técnicas (CONICET), Godoy Cruz 2290, C1425FQB Ciudad Autónoma de Buenos Aires, Argentina

**Received:** 12 June 2017
**Accepted:** 5 October 2017
**Published online:** 12 October 2017



## ABSTRACT

An iterative refining method using FullProf software (Rietveld refinement) as a multi-input–output black-box with cyclic feedback is proposed in order to accurately measure the lattice misfit in two-phase coherent alloys. The method uses two X-ray diffraction spectra taken on the same powder sample. In addition, it requires the volumetric fraction of the phases and the size of the crystallite in the precipitated phase as derived from the measurements made by the transmission electron microscopy–energy dispersive spectroscopy technique. The measurement of the lattice misfit in a $Fe_2AlV$-strengthened ferritic $Fe_{76}Al_{12}V_{12}$ alloy is shown as an application of the method.

## Introduction

Most metallic alloys are strengthened by the introduction of defects such as precipitates formed in a phase separation process. The composition, size and distribution of these precipitates are decisive for the actual mechanical properties of the alloy. These attributes of the desired phase-separated microstructure is, in general, obtained by interrupting the phase transformations, i.e. by interrupting the heat treatments, and hence it is almost always in a metastable (non-equilibrium) state from the thermodynamic point of view. Such an interesting and unstable microstructure could potentially change to some other thermodynamically stable microstructure by decreasing its energy state. At the same time, the useful properties are gradually lost during such structural change.

When the phase-separated structure containing precipitates exhibits useful properties, the precipitates are frequently coherent with respect to the matrix. In such a case, there is an elastic strain energy arising from the lattice misfit between the precipitate and the matrix. This elastic strain energy is added to the free energy of the alloy and greatly influences the kinetics of nucleation, growth, and coarsening, as well as the stability and dissolution of precipitates

Address correspondence to E-mail: ferreiros@cnea.gov.ar



DOI 10.1007/s10853-017-1682-5

under various conditions of temperature and applied load.

A typical example of systems with phase-separated microstructure elastically constrained is the $\gamma/\gamma'$ microstructure in some superalloys [1, 2], where $\gamma'$ precipitates having ordered f.c.c. structure are finely dispersed in the $\gamma$ matrix having disordered f.c.c. structure. Among other several examples we want to introduce in particular the cases of the A2/B2 and A2/$L2_1$ microstructures in the Fe-base alloys [3–5], where B2 or $L2_1$ precipitates with ordered b.c.c. structure are dispersed in the A2 matrix which has a disordered b.c.c. structure. The behaviour of B2 or $L2_1$ precipitates is essentially the same as that of $\gamma'$ precipitates in superalloys regardless of the difference in crystal structure.

The superalloys are used in load-bearing structures to the highest homologous temperature compared with any common alloy system [1]. However, due to the high material cost of superalloys, their main application is in the hot sections of turbine engines. Other demanding applications of a structural material are those in the hot sections of boilers. Ferritic steels strengthened by carbides are preferred compared to superalloys and austenitic steels for use in boiler components, especially for heavy sections, because of their low coefficient of thermal expansion, high thermal conductivity and relatively low cost [6]. However, the coarsening behavior of the incoherent strengthening carbides limits the application of ferritic steels to temperatures below 873 K. In order to increase the steam temperatures and pressures, new advanced ferritic steels with better creep resistance are needed. The current approaches to achieving this goal include a second phase (B2 or $L2_1$) precipitate strengthening [7–11].

Since superalloys and B2(or $L2_1$)-strengthened ferritic Fe-based alloys are designed for high temperature applications, the relationship between lattice misfit and creep or microstructural stability are commonly investigated [12–18].

The characterization of the lattice misfit between two phases can be obtained by several experimental techniques such as X-ray diffraction (XRD), neutron diffraction, convergent-beam electron diffraction (CBED) and evaluation of interfacial dislocation networks. All these experimental techniques, with the exception of the latter, are today widely used (e.g. [15, 19–22]).

In the more classical X-ray or neutron diffraction characterization, the lattice parameters of the phases are obtained from the quantification of powder diffraction data and then the lattice misfit is calculated. In that XRD pattern, the contribution from the precipitate phase consists of both superlattice and fundamental reflections, whereas the contribution from the matrix phase contains fundamental reflections only. In most two-phase coherent alloys the similarity between the crystal structures and lattice parameters of the both phases results in overlapping fundamental reflections. Coupled with large intrinsic line widths, this can make unambiguous determination of the contributions of the precipitate and matrix within the fundamental reflections difficult. In addition, the intensities of the superlattice reflections are in most cases weak and that weakness worsens when the volumetric fraction of the precipitated phase is low. However, the so-called single-peak quantification method is often employed (e.g. [15, 23–25]). This method is based on the separation of the convolution peak in the contribution of each phase and then calculates its lattice parameters. The deconvolution method assumes that the intensity of the separated peaks is representative of the amount of the individual phases, but this is not necessarily the case due phase-dependant factors which affect the relative intensities [26]. To improve the accuracy of the quantification some researchers used a whole pattern methods which rely on the fitting of a wide range diffraction data with a model pattern formed from the summation of individual phase components that have been calculated from crystal structure information [20]. The oldest whole pattern method was proposed 50 years ago by Rietveld [27, 28], while this technique was initially developed for the refinement of crystal structures, other parameters that must be refined to ensure best fit between the observed and calculated patterns contain useful, non-structural information that can be of interest to the analyst. These include peak width and shape, which can be related to crystallite size and strain, and the Rietveld scale factor, which, in a multiphase mixture, relates to the amount of the phase present. The Rietveld refinement method is nowadays implemented in several software as FullProf [29], DBWS [30], and GSAS [31].

Even when the Rietveld method has proven extracting the maximum available information from a powder diagram with groups of overlapping peaks,

its application to refine the superalloy XRD spectrum has two additional drawbacks such as the mixing of phases with similar crystal structures and lattice parameters together with separate peaks of very low intensity. With this ratio of intensities between the separated peaks and the overlapping peaks, the least squares refinement procedure inherent to the Rietveld method tends to ignore the volume fraction of the precipitated phase. Therefore, a different adjustment procedure should be adopted.

This work proposes an iterative refining method using FullProf software as a multi-input–output black-box with cyclic feedback working on two XRD scans taken on the same sample. Details are given of data-collection strategy, the implementation of the iterative refining process and an application to measure the lattice misfit in a $Fe_2AlV$-strengthened ferritic $Fe_{76}Al_{12}V_{12}$ alloy which microstructure consists of a ferritic matrix A2 with a dispersion of precipitates $L2_1$ ($Fe_2AlV$).

## The iterative refining method

The method requires two XRD scans on the same powder sample. It is very important for the precision of the method that the geometry of the diffractometer does not change between the two scans, i.e. that the powder sample does not move in the sample holder and no accessories are changed. The first XRD scan (named here as spectrum or pattern A) is a classical $2\theta$ wide range measurement containing the weak superlattice peaks and several strong diffraction peaks corresponding to fundamental overlapping reflections from the precipitate and matrix. The second XRD scan (named here as spectrum or pattern B) should be performed in a narrow $2\theta$ range, inside to the $2\theta$ range of the spectrum A, that include several high intensity superlattice reflections but no fundamental reflections. The weakness of superlattice reflections needs a large counting time in this second scan to achieve a high signal-to-noise ratio allowing a reliable peaks fitting.

To refine the crystal cell parameters of the precipitate and matrix, the method performs an iterative process of profile refining over each pattern collected in the aforementioned scans. The iterative process involves the use of refined parameters output from one pattern as input parameters of the other. This refinement with cyclic feedback ends when the refined parameters of both patterns reach convergent values.

As in any refinement process, the greater the number of known data in the system, the smaller the number of variables to refine and more reliable should be their refined values. In the characterization of superalloy systems, there is data usually accessed accurately by TEM and in situ (EDS) technique: the average precipitate size and the chemical composition of matrix, precipitate and bulk alloy. Therefore, assuming that the crystallite size of the precipitated phase resembles its mean size and that the volume fractions of phases can be calculated from the composition data, these two values can be used to reduce the number of variables to be refined. In addition, it is suggested also to fix the set of parameters describing the peak broadening dependence with scattering angle [32]. These parameters values can be obtained refining the diffraction pattern acquired from a powder standard [33].

Before starting the iterative refining method proposed herein, it may be useful to know approximate values for all parameters required to refine the spectra A and B with the exception of the parameters mentioned above. This can be accomplished running Fullprof software in a classical but uncoupled way on both spectra A and B. Recommendations for the refinement strategy can be seen in the recent work of Zhan et al. [34].

In Fig. 1, the iterative refining process is represented as a black-box model with cyclic feedback. The Fullprof software has been considered as a multi-input–output black-box, it works first on the XRD pattern A containing multiple peaks generated by both phases and then on the XRD pattern B containing the highest intensity superlattice peaks coming from the precipitate phase. Throughout all Rietveld refinements undertaken in this iterative process, the feedback variables are: the crystal lattice parameter of precipitate ($a_{pp}$) and the instrumental parameters: transparency (SyCos) and displacement (SySin).

The instrumental parameters (SyCos) and (SySin) affect the peak positions of the refined pattern on the $2\theta$ axis, i.e., to the lattice parameters of the matrix and precipitate. As their names suggest, both parameters shift the refined patterns with a $2\theta$ systematic sinusoidal dependence. Thus, precise refinement of them requires several diffraction peaks in the measured $2\theta$ range. This is so in the case of the spectrum A but not

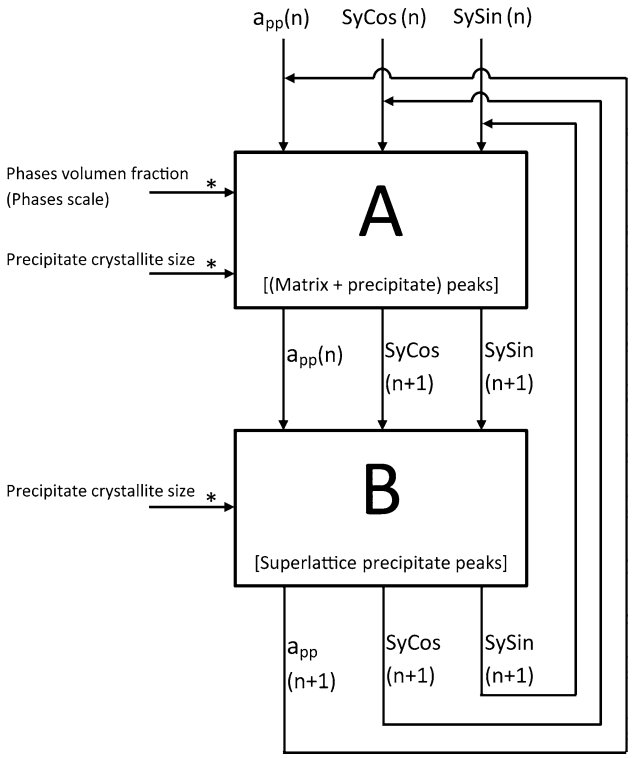


**Figure 1** Black-box model of the iterative refining process. Only the input and output data that are more relevant for the proposed refining method are indicated. Arrows marked with an asterisk point out data input accessed from TEM and EDS characterization of the alloy microstructure. The integer $n$ indicates the cycle number.

in the spectrum B. However, the experimental conditions listed above assure that the instrumental parameters are the same in the spectra A and B, therefore, we can use the values (SyCos) and (SySin) refined in spectrum A as fix input to refine spectrum B within the same refining cycle.

The implementation of the iterative refining method, as shown in Fig. 2, is formed by the following steps:

*Step 1* Set the initial value for each iterative process variable. These are: the number of black-box model cycle run, "$n$", the tolerance value defining convergence in the lattice parameter of precipitate phase, "tol", and the number of cycles defining a lasting decreasing trend of this convergence, "$N^*$".

*Step 2* In an auxiliary file all the parameters to be refined in the iterative process are stored as dynamic variables. The parameters not involved in the feedback loop are grouped and named $x_i^{A\,or\,B}{}_{(n)}$ (The parameters include in both sets are: background parameters; peak shape and asymmetry parameters; microstructural (strain effects) parameters and temperature factors. The crystal lattice parameter of the matrix belong only to the set $x_i^A{}_{(n)}$). The initial value of the dynamic variables, except for the $x_i^B$ variables, are the values found in the previous and disjoint run of the software Fullprof on the spectrum A. The $x_i^B$ values are found running the software Fullprof on the spectrum B holding fixed the values of the parameters, $\mathrm{SyCos}^B = \mathrm{SyCos}^A$, $\mathrm{SySin}^B = \mathrm{SySin}^A$ and $a_{\mathrm{pp}}^B = a_{\mathrm{pp}}^A$.

*Step 3* Write the input control file of Fullprof software (''pcr'' file) to refine the spectrum A with the respective values from the auxiliary file. Indicate that the $a_{\mathrm{pp}}$ parameter should not be refined. Run Fullprof software to refine the spectrum A. Rewrite the auxiliary file with the results of the refinement.

*Step 4* Write the input control file of Fullprof software (''pcr'' file) to refine the spectrum B with the respective values from the auxiliary file. Indicate that the $a_{\mathrm{pp}}$ parameter should be refined, but not the SyCos and SySin parameters. Run Fullprof software to refine the spectrum B. Rewrite the auxiliary file with the results of the refinement.

*Step 5* If the parameter $a_{\mathrm{pp}}$ is convergent during $N$ cycles and it is not greater than $N^*$, then, go back to Step 3, otherwise, calculate the $a_{\mathrm{pp}}$ final value as its average in the last two $n$ cycles and terminate the operation.

## Application and discussion

This paper chooses an aged $Fe_{76}Al_{12}V_{12}$ (at.%) alloy as the experimental data for an application of the iterative refining method. This alloy has been characterized in Ref. [35] and, as was mentioned in the introduction of this paper, its microstructure consists of a ferritic matrix A2 with a dispersion of precipitates $L2_1$ ($Fe_2AlV$). The size and distribution of these precipitates can be carefully controlled during processing and subsequent heat treatments to optimize mechanical performance. There is interest in adding others elements to its composition to improve the properties at high temperature, but could strongly affect the lattice misfit between matrix and

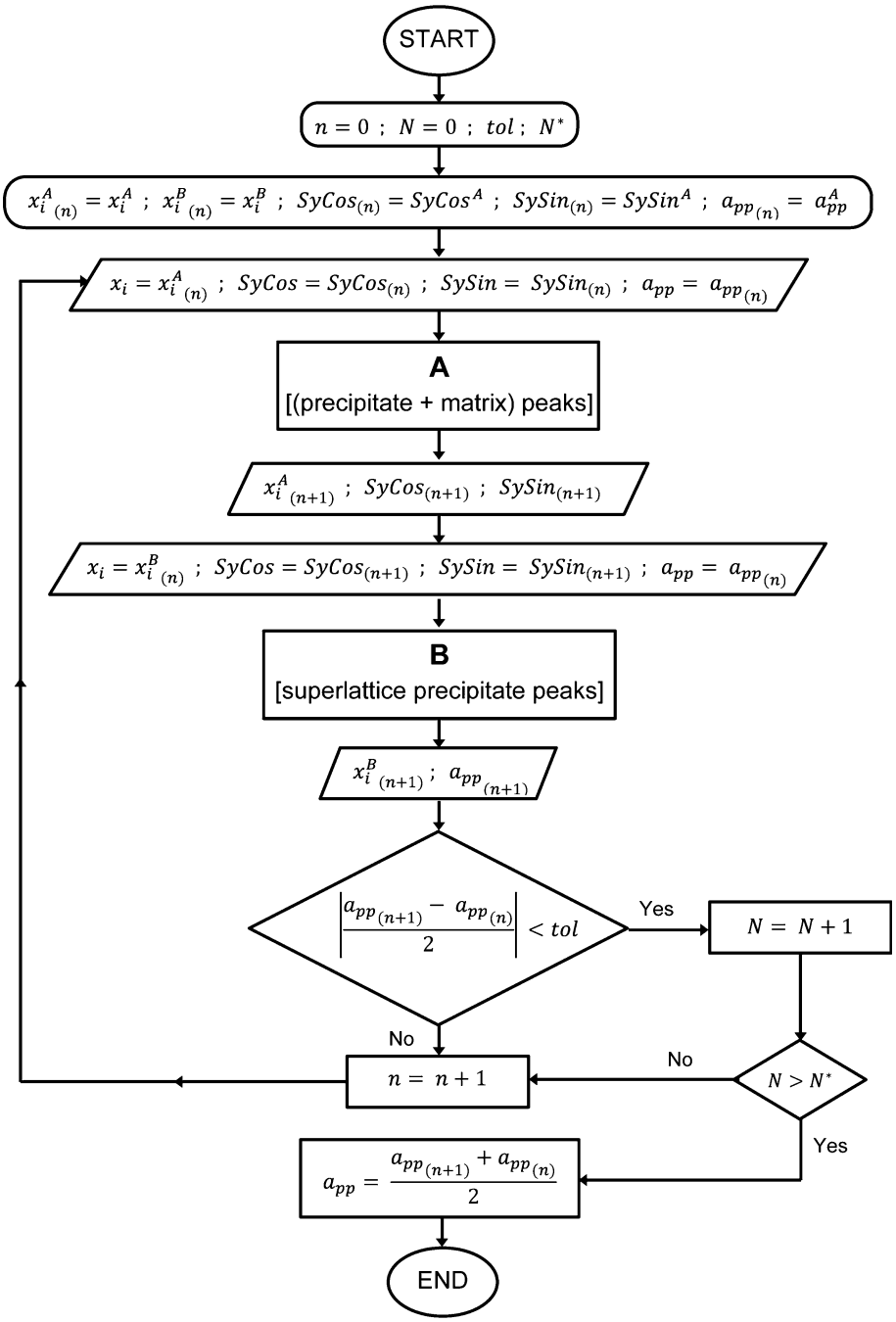


**Figure 2** Flowchart of the iterative refining process. Data input accessed from TEM and EDS characterization of the alloy microstructure is left aside in the drawing.

precipitates and hence change the interfacial coherency with consequent instability in precipitate morphology and size. Therefore, the characterization of the variation in the lattice misfit with the addition of others elements seems to be useful.

The alloy ingot was melted in an electric arc furnace using a tungsten electrode and a water cooled copper crucible under argon atmosphere. The ingot was then heated in an electric furnace under argon atmosphere up to 1100 °C for 136 h and hot rolled in several passes to form a plate with about 3 mm thickness. In Ref. [35] a piece of this plate was subjected to a 15 min solution heat treatment at 1100 °C followed by an aging treatment at 700 °C for 22 min to obtain a fine distribution of spherical precipitates. The characterization of this microstructure using TEM-EDS analysis gave the following results: 20.4 nm mean diameter of the precipitate (the

standard deviation of the diameters distribution is 7.7 nm) and volume fraction of 0.218 ± 0.013 (details of the measurements procedure are given in [35]). In the current work, another piece of the hot rolled plate was filed with a diamond file and then the powder was sieved to obtain a particle size of less than 90 μm. The filing operation may contaminate the powder with particles from the used tool; however there were no indications of unexpected phases in our XRD measurements. Previous to XRD characterization, the powder was embedded in a Tantalum container inside a quartz tube which was evacuated and subjected to a thermal cycle that replicates the solution + aging heat treatment given to the whole piece in Ref. [35]. This heat treatment, besides replicating the microstructure, induces the relieving of residual stresses generated by the filing operation in the powder grains. The XRD patterns from powder were taken on a Panalytical Empyrean X-ray diffractometer (Cu Kα radiation) mounted in the Bragg–Brentano configuration and equipped with PIXcel$^{3D}$ detector. The data were collected in two scans. First, a type A scan in angular range $20° \leq 2\theta \leq 120°$ with total collect time of 7200 s and angular step of 0.026° (1.87 s/step). In order to improve statistics in the angular range where the most intense superlattice reflection of $L2_1$ phase occur ($29° \leq 2\theta \leq 33°$), a type B scan was performed with the same total collect time and angular step than in scan A increasing the counting time per step to 46.75 s/step. Figure 3 shows the two different XRD scans. All observable reflections in scan A show double peaks due to $K_1^{\alpha}$ and $K_2^{\alpha}$ radiation, but in the observable reflection of scan B the large width of the peaks causes them to overlap and look like a single symmetrical peak. The five observable peaks in the Fig. 3a have contributions of reflections coming from A2 and $L2_1$ phases (see black and red marks at nearby Bragg positions in Fig. 3a) but, hidden in the background, there are several peaks corresponding to reflections of $L2_1$ superlattice (isolated double red marks in Fig. 3a). As expected, the largest of these is the reflection (200) located approximately in $2\theta \approx 31°$ as can be seen from the data collected in scan B (Fig. 3b).

Prior to start the Rietveld refinement of the diffraction data, we characterized the instrumental broadening using the diffraction patterns acquired in the same angular range with a silicon standard. When fitting $Fe_{76}Al_{12}V_{12}$ diffraction patterns, the calculated instrumental broadening was convoluted with the Thompson–Cox–Hastings Pseudo-Voigt [36, 37] peak profile provide in the FullProf program. The space groups of A2 and $L2_1$ phases are $Im\bar{3}m$ (229) and $Fm\bar{3}m$ (225) respectively [38, 39] and, because both structure are cubic, the three edges of the crystals structures are set equals and defined for a single parameter in the refining process. In Fig. 3 the diffraction pattern determined from the Rietveld refinement (Ycalc) is superimposed onto the experimentally acquired diffraction patterns (Yobs). In addition, two insets in Fig. 3a show the contributing constituents of the A2 and $L2_1$ phases to the summed diffraction signal in the fundamental (110) reflection and the quality of the refinement pondered by the $R$ and $\chi^2$ (Chi2) factors [27].

The Fig. 4 shows the evolution of the precipitate lattice parameter $(a_{pp} = a_{L2_1})$ and the instrumental (SyCos) and (SySin) parameters through the cycles of the iterative process. In the three graphs the dotted line point out the values of these parameters as obtained from the spectrum A after a classical refinement with the FullProf software using the restrictions over the crystallite size of the precipitated phase and the volume fractions of phases. As can be observed, in the third operation cycle $(n = 3)$ the three parameters reach the convergence and hold this lasting decreasing trend during $N = 3$ cycles $(N^* = 2)$. The influence of the spectrum B data on the refined value of the lattice parameter of the precipitated phase is greater than 0.14%. The meaning of this result may be more appreciated if it is analyzed in the context of the lattice misfit ($\delta$) between the two phases. The equation for calculating the lattice misfit was adapted from the one that is commonly used for $\gamma'$ strengthened superalloys [40]:

$$\delta = \frac{2(a_{L2_1} - 2a_{A2})}{a_{L2_1} + 2a_{A2}}$$

Here, the lattice parameters of $\gamma$ and $\gamma'$ phases were substituted by those of the A2 and $L2_1$ phases. Additionally, a factor of two was introduced to take account for the difference in unit cell size. Figure 5 displays the evolution of the lattice misfit during the iterative process, the positive value obtained with the isolated refinement of the spectrum A becomes a negative number during the iterative refinement between the spectra A and B. And so, the interpretation of mechanical properties would be strongly

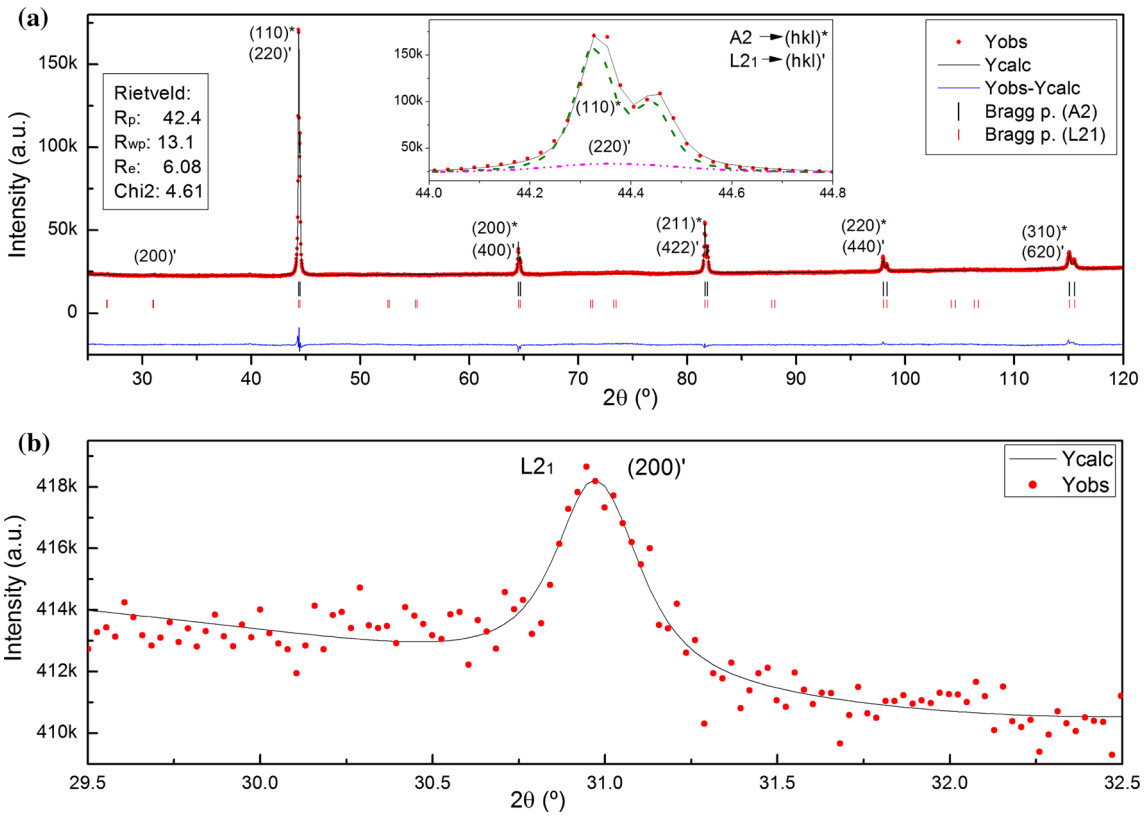


**Figure 3** XRD powder diffraction spectra obtained from the $Fe_{76}Al_{12}V_{12}$ (at.%) alloy after 15 min solution heat treatment at 1100 °C followed by an aging treatment at 700 °C for 22 min. **a** The fitted diffraction pattern obtained with the iterative refinement process, along with the intensity contributions of the A2 and $L2_1$ phases, is shown. The intensity contributions of each phases in the fundamental (110) reflection is also highlighted in the inset graph (dotted lines). **b** Measured range with increased total counts containing the most intense (200) reflection of the $L2_1$ phase superlattice and its fitted pattern.

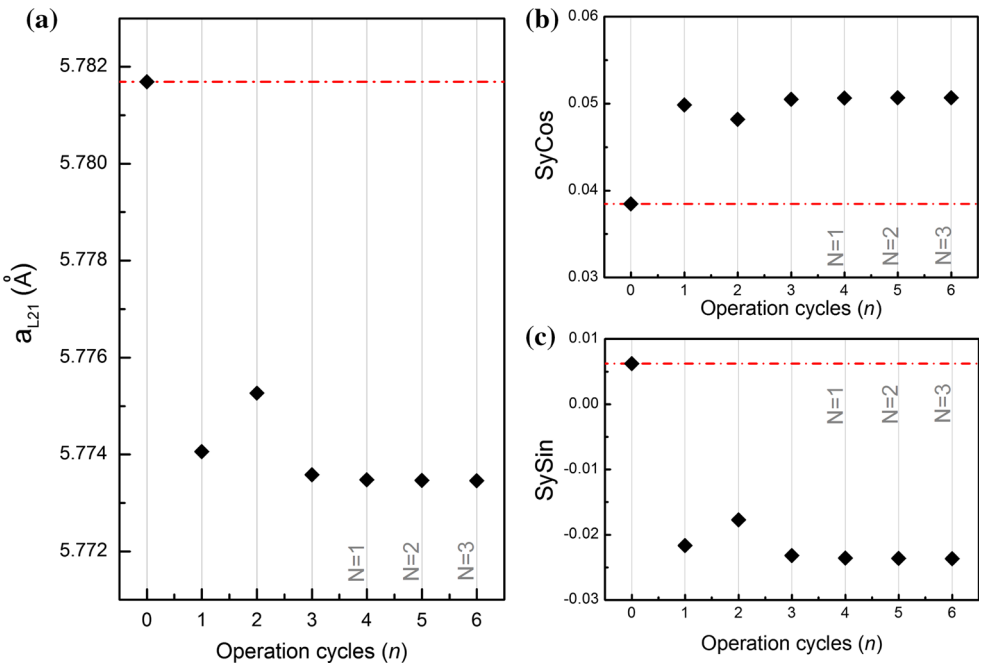


**Figure 4** Evolution of the feedback parameters through the cycles of the iterative process.

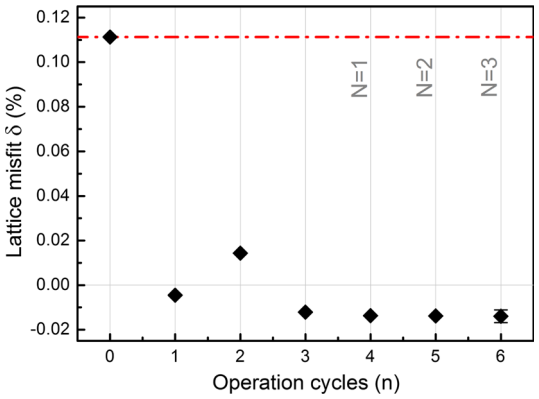


**Figure 5** Lattice misfit evolution through the cycles of the iterative process.

dependent on which of these results is used. To increase the credibility of our results, the volume fraction was given the status of a free variable in the iterative refining procedure after the last stage of convergence and it was noted that it remain in a realistic value of $0.207 \pm 0.005$. The difference between $\delta$ values obtained with restricted and free volume fraction defines the confidence interval for the lattice misfit as illustrated in Fig. 5. As shown, the scatter in $\delta$ is significantly lower than its variation during the first stage of convergence.

## Conclusions

An iterative refining method using FullProf software as a multi-input–output black-box with cyclic feedback has been proposed in this paper. The scope of the method is to accurately measure the lattice misfit in superalloys using two XRD scans on the same sample. It works first on a widespread XRD pattern containing multiple peaks generated by both, precipitate and matrix, phases and then on a narrow XRD pattern with better statistic containing the highest intensity superlattice peak coming from the precipitate phase. The feedback parameters are the lattice parameter of the precipitate phase and the Transparency and Displacement instrumental parameters. Two refinement parameters are restricted in their values to measurements made by TEM-EDS; they are volume fraction of the phases and size of crystallite in the precipitated phase. The improvement of accuracy comes from the feedback of the precipitate lattice parameter refined with data where the signal-to-noise ratio is high and the superlattice diffraction peaks of precipitate phase are isolated; this feedback is possible because the instrumental parameters are the same in the two XRD scans involved in the experimental arrangement of the method.

## Acknowledgements

The authors wish to thank Dr. Daniel Vega for the services provided by the Difracción de Rayos X Laboratory, Física de la Materia Condensada Department, Gerencia de Investigaciones y Aplicaciones, GAIyANN-CAC-CNEA. PAF was supported by a Comisión Nacional de Energía Atómica (CNEA) professional fellowship.

## Compliance with ethical standards

**Conflict of interest** The authors declare that they have no conflict of interest.

## References

[1] Reed RC (2006) The superalloys fundamentals and applications. Cambridge University Press, Cambridge

[2] Mughrabi H (2009) Microstructural aspects of high temperature deformation of monocrystalline nickel base superalloys: some open problems. Mater Sci Technol 25:191–204

[3] Hao SM, Takayama T, Ishida K, Nishizawa T (1984) Miscibility gap in Fe–Ni–Al and Fe–Ni–Al–Co systems. Metall Trans A 15:1819–1828

[4] Mendiratta MG, Ehlers SK, Lipsitt HA (1987) $DO_3$-B2-alpha phase relations in Fe–Al–Ti alloys. Metall Trans A 18:509–518

[5] Maebashi T, Kozakai T, Doi M (2004) Phase equilibria in iron-rich Fe–Al–V ternary alloy system. Z Met 95:1005–1010

[6] Bhadeshia HKDH (2001) Design of ferritic creep-resistant steels. ISIJ Int 41:626–640

[7] Stallybrass C, Sauthoff G (2004) Ferritic Fe–Al–Ni–Cr alloys with coherent precipitates for high-temperature applications. Mater Sci Eng A 387–389:985–990

[8] Vo NQ, Liebscher CH, Rawlings MJS, Asta M, Dunand DC (2014) Creep properties and microstructure of a precipitation-strengthened ferritic Fe–Al–Ni–Cr alloy. Acta Mater 71:89–99

[9] Krein R, Palm M, Heilmaier M (2009) Characterization of microstructures, mechanical properties, and oxidation

behavior of coherent A2 + $L2_1$ Fe–Al–Ti. J Mater Res 24:3412–3421

[10] Ferreirós PA, Alonso PR, Gargano PH, Bozzano PB, Troiani HE, Baruj A, Rubiolo GH (2014) Characterization of microstructures and age hardening of $Fe_{1-2x}$ $Al_xV_x$ alloys. Intermetallics 50:65–78

[11] Senčekova L, Palm M, Pešička J, Veselý J (2016) Microstructures, mechanical properties and oxidation behaviour of single-phase Fe3Al(D03) and two-phase α-Fe, Al(A2) + Fe3Al(D03) Fe–Al–V alloys. Intermetallics 73:58–66

[12] Calderon HA, Fine ME, Weertman JR (1988) Coarsening and morphology of $\beta'$ particles in Fe–Ni–Al–Mo ferritic alloys. Metall Trans A 19:1135–1146

[13] Svoboda J, Lukáš P (1998) Model of creep in <001> -oriented superalloy single crystals. Acta Mater 46:3421–3431

[14] Onaka S, Kobayashi N, Fujii T, Kato M (2003) Energy analysis with a superspherical shape approximation on the spherical to cubical shape transitions of coherent precipitates in cubic materials. Mater Sci Eng A 347:42–49

[15] Maebashi T, Doi M (2004) Coarsening behaviours of coherent $\gamma'$ and $\gamma$ precipitates in elastically constrained Ni–Al–Ti alloys. Mater Sci Eng A 373:72–79

[16] Heckl A, Neumeier S, Göken M, Singer RF (2011) The effect of Re and Ru on $\gamma/\gamma'$ microstructure, γ-solid solution strengthening and creep strength in nickel-base superalloys. Mater Sci Eng A 528:3435–3444

[17] Mughrabi H (2014) The importance of sign and magnitude of $\gamma/\gamma'$ lattice misfit in superalloys-with special reference to the new $\gamma'$-hardened cobalt-base superalloys. Acta Mater 81:21–29

[18] Long H, Wei H, Liu Y, Mao S, Zhang J, Xiang S, Chen Y, Gui W, Li Q, Zhang Z, Han X (2016) Effect of lattice misfit on the evolution of the dislocation structure in Ni-based single crystal superalloys during thermal exposure. Acta Mater 120:95–107

[19] Pyczak F, Neumeier S, Göken M (2009) Influence of lattice misfit on the internal stress and strain states before and after creep investigated in nickel-base superalloys containing rhenium and ruthenium. Mater Sci Eng A 510–511:295–300

[20] Collins DM, Yan L, Marquis EA, Connor LD, Ciardiello JJ, Evans AD, Stone HJ (2013) Lattice misfit during ageing of a polycrystalline nickel-base superalloy. Acta Mater 61:7791–7804

[21] Collins DM, D'Souza N, Panwisawas C (2017) In-situ neutron diffraction during stress relaxation of a single crystal nickel-base superalloy. Scr Mater 131:103–107

[22] Brunetti G, Settefrati A, Hazotte A, Denis S, Fundenberger J-J, Tidu A, Bouzy E (2012) Determination of $\gamma$-$\gamma'$ lattice misfit in a single-crystal nickel-based superalloy using convergent beam electron diffraction aided by finite element calculations. Micron 43:396–406

[23] Mukherji D, Gilles R, Barbier B, Del Genovese D, Hasse B, Strunz P, Wroblewski T, Fuess H, Rösler J (2003) Lattice misfit measurement in Inconel 706 containing coherent $\gamma'$ and $\gamma''$ precipitates. Scr Mater 48:333–339

[24] Sugui T, Minggang W, Huichen Y, Xingfu Y, Tang L, Benjiang Q (2010) Influence of element Re on lattice misfits and stress rupture properties of single crystal nickel-based superalloys. Mater Sci Eng A 527:4458–4465

[25] Zenk CH, Neumeier S, Stone HJ, Göken M (2014) Mechanical properties and lattice misfit of $\gamma/\gamma'$ strengthened Co-base superalloys in the Co–W–Al–Ti quaternary system. Intermetallics 55:28–39

[26] Madsen C, Scarlett NVY (2008) Quantitative Phase Analysis. In: Dinnebier RE, Billinge SJL (eds) Powder diffraction theory and practice. The Royal Society of Chemistry, Cambridge, pp 298–329

[27] Rietveld HM (1967) Line profiles of neutron powder-diffraction peaks for structure refinement. Acta Cryst A 22:151–152

[28] Rietveld HM (1969) A profile refinement method for nuclear and magnetic structures. J Appl Cryst 2:65–71

[29] Rodriguez-Carbajal J (1993) Recent advances in magnetic structure determination by neutron powder diffraction. Phys B 192:55–69

[30] Young RA, Sakthivel A, Moss TS, Co Paiva-Santos (1995) DBWS-9411—an upgrade of the DBWS*.* programs for Rietveld refinement with PC and mainframe computers. J Appl Cryst 28:366–367

[31] Larson AC, Von Dreele RB (2004) General structure analysis system (GSAS), Los Alamos National Laboratory Report LAUR 86-748, University of California

[32] Hammond C (2009) The basic of crystallography and diffraction, 3rd edn. Oxford University Press, IUCr

[33] Rodríguez-Carvajal J (2001) An introduction to the program FullProf 2000. Laboratoire Léon Brillouin, France

[34] Zhan W-P, Zhang H-R, Li Q, Zhu Y-H, Feng Z-J, Gao H-H, Shen W-F, Wu P, Ding G-T, Cao M (2015) Automated method for varying the order in which parameters are refined in powder diffraction. Comput Mater Sci 107:210–215

[35] Ferreirós PA, Alonso PR, Rubiolo GH (2017) Coarsening process and precipitation hardening in $Fe_2$AlV-strengthened ferritic $Fe_{76}Al_{12}V_{12}$ alloy. Mater Sci Eng, A 684:394–405

[36] Thompson P, Cox DE (1987) Hastings JB Rietveld refinement of Debye–Scherrer synchrotron X-ray data from $Al_2O_3$. J Appl Cryst 20:79–83

[37] Finger LW (1998) PROFVAL: functions to calculate powder-pattern peak profiles with axial divergence asymmetry. J Appl Cryst 31:111

[38] Palm M, Inden G, Thomas N (1995) The Fe–AI–Ti System. J Phase Equilib 16:209–222

[39] Vasundhara M, Srinivas V, Rao VV (2008) Evidence for cluster glass behavior in $Fe_2VAl$ Heusler alloys. Phys Rev B 78(064401):1–10

[40] Reed RC, Rae CMF (2014) Physical metallurgy of the nickel-based superalloys. In: Laughlin DE, Hono K (eds) Physical metallurgy, vol 3, 5th edn. Elsevier, Amsterdam, pp 2215–2290